ELSEVIER

Agricultural and Forest Meteorology 109 (2001) 249–263

AGRICULTURAL AND FOREST METEOROLOGY

www.elsevier.com/locate/agrformet

A comparison of digital and film fisheye photography for analysis of forest canopy structure and gap light transmission

Gordon W. Frazer [a,*], Richard A. Fournier [b,1], J.A. Trofymow [c,2], Ronald J. Hall [d,3]

[a] *Department of Geography, University of Victoria, P.O. Box 3050, Victoria, BC, Canada V8W 3P5*
[b] *Natural Resources Canada, Canadian Forest Service, Laurentian Forestry Centre, P.O. Box 3800, 1055 du P.E.P.S., Sainte-Foy, Que., Canada G1V 4C7*
[c] *Natural Resources Canada, Canadian Forest Service, Pacific Forestry Centre, 506 West Burnside Road, Victoria, BC, Canada V8Z 1M5*
[d] *Natural Resources Canada, Canadian Forest Service, Northern Forestry Centre, 5320-122 Street, Edmonton, Alta., Canada T6H 3S5*

Received 15 February 2001; received in revised form 14 July 2001; accepted 16 July 2001

Abstract

Due to the scarcity and high cost of conventional film-based hemispherical photographic systems, some forest scientists are now using multi-purpose, consumer-grade digital cameras for the analysis of forest canopy structure and gap light transmission. Although the low cost of digital cameras and direct capture of digital images appear to offer significant advantages over film camera systems, relatively little is known about their technical differences from an applications perspective. In this study, we compared the performance of a popular digital camera (Nikon Coolpix 950 with FC-E8 fisheye) with a conventional film camera (Nikon F with Nikkor 8 mm fisheye) under different stand structures and sky conditions. Our findings show that the Nikon Coolpix 950 digital camera produced hemispherical canopy photos with substantial color blurring towards the periphery of the exposure. We believe that chromatic aberration associated with the camera's lens optics may be the source of this phenomenon; however, other factors may have also contributed to the diminished image sharpness. Color blur influenced (i) the size, shape, and distribution of canopy gaps; (ii) the accuracy of edge detection and the binary division of pixels into sky and canopy elements, and (iii) the magnitude, range, and replication of canopy openness, leaf area, and transmitted global radiation results. The Nikon Coolpix 950 produced canopy openness measures that were 1.4 times greater than film estimates in 22 of the 36 photo pairs. Cloud cover and sky brightness also influenced the spectral characteristics of the lateral chromatic aberration (halos), and thus had an added and unpredictable effect on canopy openness. Setting the Nikon Coolpix 950 to record in black and white, and shooting only under uniformly overcast skies will help to minimize the unpredictable effects of chromatic aberration. Nevertheless, we recommend a cautious approach when undertaking canopy measurements with the Nikon Coolpix 950, particularly when stands are dense and canopy openness falls below 10%. High-quality (1:4) JPEG compression had no significant influence on mean canopy openness; however, lower XGA and VGA image resolutions

*Corresponding author. Tel.: +1-250-656-4852; fax: +1-250-721-6216.
E-mail addresses: gfrazer@uvic.ca (G.W. Frazer), rfournier@cfl.forestry.ca (R.A. Fournier), ttrofymow@pfc.cfs.nrcan.gc.ca (J.A. Trofymow), rhall@nrcan.gc.ca (R.J. Hall).
[1]Present address: CARTEL, Départ. de Géographie et Télédétection, Univ. de Sherbrooke, Sherbrooke, QC, Canada, J1K 2R1. Tel.: +1-819-821-8000/ext. 3209; fax: +1-819-821-7944.
[2]Tel.: +1-250-363-0677.
[3]Tel.: +1-780-435-7209.

PII: S0168-1923(01)00274-X

combined with 1:4 JPEG compression produced mean canopy openness results that were significantly lower than openness data extracted from uncompressed, full-resolution TIFF photos.

Keywords: Hemispherical canopy photography; Leaf area index; Canopy structure; Forest canopies; Fisheye photography; Digital photography; Canopy openness; Light transmission; Gap light analyzer

1. Introduction

Forest canopy structure constitutes the complex spatial arrangement of foliage, branches, and the boles of trees, and it has been a significant focus of research because of its influence on a wide range of biophysical and ecological processes (Perry, 1994; Parker, 1995; Spies, 1998). The relationship between canopy structure and the temporal and spatial distribution of incident understory light has been a particular interest of forest ecologists studying the effects of natural disturbance, forest succession, timber harvesting, and silvicultural prescriptions on the survival, pattern, and diversity of understory plants and trees (e.g. Canham et al., 1990, 1994; Gray and Spies, 1996; Wright et al., 1998; Nicotra et al., 1999).

Numerous ground-based optical tools and techniques have been developed to measure attributes of forest canopy structure (for instance, openness, leaf area, and foliage inclination angle) and the quantity and quality of incident understory light (Welles and Cohen, 1996; Gendron et al., 1998; Jennings et al., 1999). One optical method that has received increased attention is hemispherical (fisheye) canopy photography, because of its unique ability to permanently record the spectral and spatial characteristics of all canopy elements, and also to rapidly predict the seasonal radiant flux of direct and diffuse light through discrete openings (gaps) in the canopy (Chazdon and Field, 1987; Canham, 1988; Rich, 1990).

Traditionally, hemispherical canopy photography has relied upon conventional black and white, or color films (negatives or diapositives), and charge-coupled device (CCD) scanners to produce digital images for analysis (Frazer et al., 1997). Today, however, high-resolution (2–3 million pixels) consumer-grade digital cameras offer forest scientists a less expensive and practical alternative to traditional film photography. At quick glance, the advantages of digital photography seem obvious. First, capturing images in digital form bypasses the added expense and time associated with photographic film, film development, and scanning. Second, the ability to preview digital images in the field would help to establish the optimal exposure settings for a given set of stand and sky conditions. Third, image processing and data extraction could occur directly in the field, thus creating a more streamlined process (this would be a particular advantage in remote sites).

Despite many of these apparent advantages, very few studies have been designed to investigate the possible drawbacks or limitations of using consumer-grade digital cameras for scientific applications like hemispherical canopy photography (e.g. Englund et al., 2000). Although both kinds of cameras (digital and analogue) are constrained by the quality of the fisheye optics, digital cameras are subject to other added sources of noise (error) related to the detector (CCD array) and supporting electronics, which could adversely affect the spectral and spatial qualities of the image (Holst, 1996). Reliable, hemispherical image processing requires photos that have sufficient spectral separation between sky and canopy elements, as well as a high degree of spatial integrity. We therefore expect that the lens optics, along with the resolution and quantum efficiency (response to different wavelengths of light) of the CCD sensor, will be a few of the key factors affecting the use of consumer-grade digital cameras in hemispherical canopy photography.

To investigate these potential concerns, we undertook a field trial to compare two popular hemispherical camera systems (one digital and one film) under clear and overcast skies and within a range closed-canopy conditions. Here, we present the results from this study, including (i) a comparison of canopy openness, effective leaf area index (L_e), and transmitted global photosynthetically active radiation (PAR) estimates derived from photographs taken with a Nikon F and Nikkor 8 mm (*f*/8) fisheye lens (film), and a Nikon Coolpix 950 and Nikkor FC-E8 fisheye converter

(digital); (ii) the influence of stand maturity class and sky conditions on digital-to-film ratios of openness, L_e, and transmitted global PAR; (iii) geometric (radial) distortion data measured for each of the camera systems; (iv) the impacts of XGA (1024 × 768 pixels) and VGA (640 × 480 pixels) resolutions, and 1:4 JPEG compression on canopy parameters computed from digital photos; (v) some considerations for using consumer-grade digital cameras in forest canopy applications.

2. Materials and methods

2.1. Study site description

The field portion of this study took place in 2 of 40 permanent coastal forest chronosequence research plots established by the Canadian Forest Service, Pacific and Yukon Region, on southern Vancouver Island, BC, Canada (Trofymow et al., 1997). Both plots belong to the Victoria watershed south (VWS) chronosequence, which is located 45 km northwest of the city of Victoria in the Sooke Lake watershed (approximately 48°34′N and 123°39′W). The VWS chronosequence is found within the coastal western Hemlock (CWH) biogeoclimatic zone and represents the drier (mean annual precipitation 1425 mm) and slightly warmer (mean annual temperature 9.4°C) eastern variant of the very dry maritime CWH subzone (CWHxm1; Green and Klinka, 1994).

The two second-growth forest stands selected for this study were markedly different in mean age, density, and height; species composition; and site orientation (Table 1). The youngest stand (immature; VWS-02) was composed of almost equal numbers of Douglas-fir (*Pseudotsuga menziesii* (Mirb.) Franco) and western Hemlock (*Tsuga heterophylla* (Raf.) Sarg.), while the older stand (mature; VWS-05) was predominantly Douglas-fir (80%), with some interspersed western redcedar (*Thuja plicata* Donn.), red alder (*Alnus rubra* Bong.), and western Hemlock. The immature stand was significantly younger (mean age, 18 years), more dense (2250 stems/ha), and shorter (mean height, 9.8 m) than the mature stand (mean age, 89 years; mean density, 693 stems/ha; mean height, 34 m). Measurements of diffuse non-interceptance (DIFN) and L_e collected at these two plots in 1995 using paired LAI-2000 plant canopy analyzers (LI-COR Inc., Lincoln, Nebraska) indicated that the mature stand was significantly more open (DIFN: 0.043 ± 0.012; L_e: $3.81 \pm 0.42\ m^2/m^2$) than the immature stand (DIFN: 0.025 ± 0.009; L_e: $4.36 \pm 0.43\ m^2/m^2$; Frazer et al., 2000a).

2.2. Sampling design

Two parallel transects, each 50 m long and separated by 10 m of distance, were established in each of the two different stands. Sample points (photo stations) were positioned every 10 m from the start to the end of these transects, creating a total of 6 stations

Table 1
Summary mensuration data for VWS plots

Stand	Latitude (N)	Longitude (W)	Elevation (m)	Slope (°)	Aspect (°)	Species[a]	*n*	Density[b] (number/ha)	Basal area[b] (m^2/ha)	DBH[b] (cm)	Height[b] (m)	Age[c] (years)
Immature	48°33′51″	123°38′55″	305	22	20	FD	24	1019	22.7	13.2	11.9	41
						HW	29	1231	7.7	6.6	7.6	
						All	53	2250	30.4			
Mature	48°33′47″	123°39′45″	240	6	315	CW	7	99	4.8	23.1	16.9	108
						DR	1	14	1.5	36.2	37.4	
						FD	39	552	81.8	39.0	34.2	
						HW	1	14	0.6	22.5	20.5	
						PW	1	14	<0.1	6.5	8.0	
						All	49	693	88.7			

[a] CW, western redcedar; DR, red alder; FD, Douglas-fir; HW, western Hemlock; PW, western white pine.
[b] Mean calculated by species.
[c] Mean calculated for all sampled trees.

per transect and 12 per stand (i.e. 2 transects having 6 stations per transect). At each station, digital and conventional film photographs were taken at virtually identical positions (1.3 m above the sample station) and times. Each camera was mounted with the lens facing skyward and the camera body leveled and aligned with magnetic north. A duplicate mounting plate affixed to each of the two camera systems facilitated the quick exchange of cameras 'on' and 'off' a single tripod, so that a series of photographs could be taken with minimal time delay (less than 2 min). A complete set of digital and film photographs was taken at each of the two plots under two contrasting sky conditions: one set of photos was taken on 6 March 2000 under relatively clear skies (<20% cloud cover), and 2 days later another set was taken under uniformly overcast skies (100% cloud cover).

2.3. Photographic equipment and exposure settings

We field tested and compared two popular camera and fisheye lens systems: the digital camera was a Nikon Coolpix 950 (firmware version 1.3) and Nikkor FC-E8 fisheye converter (combined focal length equivalent to 7.2 mm, and the combined *F* number is *f*/2.4), and the conventional film camera was a Nikon F and Nikkor 8 mm *f*/8 fisheye lens. The Nikon Coolpix 950 uses a high-density 1/2″ color CCD sensor, with a total and effective pixel count of 2.11 and 1.92 million pixels (1600 × 1200 pixels), respectively. The Nikon F was loaded with Fujicolor NPH 400 Professional negative color film.

Our methods of exposure were different for each of the cameras because of inherent differences in lens speed, film (ISO 400) and detector (ISO 80) sensitivity, and exposure control. Unlike the Nikon F, the digital camera did not allow full manual control of both the shutter speed and lens aperture. We therefore set the autofocus, exposure mode, and *f*-stop of the digital camera to infinity, aperture priority (shutter speed is set automatically by the camera), and *f*/2.6, respectively. We chose the widest lens aperture because of the limited ISO sensitivity of the CCD, and also so that the camera would automatically shoot at higher shutter speeds, thereby minimizing any image defects (blurring) created by movement in the canopy, or by the random motion (jitter) associated with manual release of the shutter (the self-timer is automatically disabled when the Nikon Coolpix 950 is in FISHEYE1 mode). In addition to these basic settings, we used the manual exposure compensation (either −0.7 or −1.0 eV) and playback capabilities of the digital camera to help optimize the exposure for each of the stand and sky conditions.

Once the optimum exposure was determined for the digital camera, we took a series of photographs at each sample point using both camera systems. With the digital camera, photographs were taken in a sequence of four separate image modes: FULL (1600 × 1200 pixels, uncompressed TIFF), FINE (1600 × 1200 pixels, 1:4 compression JPEG), XGA (1024 × 768 pixels, 1:4 compression JPEG), and VGA (640 × 480 pixels, 1:4 compression JPEG). Exposing the photographic film with the Nikon F was far simpler: based on previous photographic work at these sites (Frazer et al., 2000a), we set the lens aperture to *f*/8 and made four separate exposures at shutter speeds of 1/125, 1/250, 1/500, and 1/1000 m/s. Eight canopy photos (four digital and four film) were therefore taken at each station. In total, we collected 384 canopy images (i.e. 8 photos per station × 12 stations per plot × 2 plots (immature and mature) × 2 sky conditions (overcast and clear)).

We marked the photographic film at the time of exposure using external lights (red-colored, 100 mcd LEDs) focused through two very fine (0.5 mm diameter) optical-grade fibers located at the edge and on either side of the outer lens optics. These markings (dots) were used during the image processing stage to identify the north/south orientation axis of the film plane, as well as the outer edge of the exposure. Similar methods to mark the digital photos were unnecessary because of the static position of the exposure within the CCD array, and the fact that both cameras were aligned on a shared tripod in precisely the same manner (i.e. the long axis of each camera body was aligned north and south, while the tops of the cameras faced west).

2.4. Measurement of radial lens distortion

Both of the fisheye lenses used in this study were designed to produce a polar projection (angular distances in the object region are proportional to radial distances on the image plane). However, previous studies show that most commercial lenses do not conform exactly to their design specifications, and

that the character and magnitude of this deviation is specific to the lens model and manufacturer (Herbert, 1987). To control for these potential between system differences, we undertook two sets of calibration tests to determine the true radial distortion and maximum field of view (FOV) for each lens: one set of tests was done in-house, while the other was completed by the Institut National d'Optique (INO) in Sainte-Foy, Que.

Our in-house calibrations were composed of three separate tests. First, we positioned the cameras on a tripod with the lens facing skyward, leveled, and at a fixed distance from a tall, multi-storied building. The building had a regular grid of windows with intersection points (window corners) that were easily identified in the digital image. To establish the precise angular distance of these object points from the camera's optical axis, we centered a precision (Nikon) optical survey station over the same location and at the same height as the camera lens, and then recorded the vertical angles to each of the window corners. The procedure was repeated at three separate distances (10, 25, and 65 m) from the building, so that we could sample a wide range of view angles and also average some of the experimental error related to the leveling and positioning of the instruments. Radial distances on the image plane were computed using the pixel coordinates of the image centre and each of the unique points (window corners) located within the image array.

The second-calibration procedure was similar in design to the first; however, for the second test we used a much shorter vertical target (2.5 m) and target distances (0.5 and 1 m). The indoor target was constructed using 6 mm circular (dots) markers placed on a plumb wall every 5 cm along a vertical line that stretched from the floor to the ceiling. The camera tripod was set square to the target, and the height of the top of the lens barrel was adjusted so that the optical axis of the lens formed a 90° angle with the centre of a marker. We used the horizontal distance between the optical axis of the lens and the target, along with the heights of the dot centers above the lens barrel, to compute an angular distance to each of the target points. Radial distances of the projected points on the image plane were measured in the same manner as described above. Dr. Daniel Mailly (Quebec Ministry of Natural Resources), following the procedures of Clark and Follin (1988), undertook our third in-house lens calibration. Lastly, independent radial distortion measurements on the Nikon Coolpix 950 and FC-E8 fisheye converter were conducted at INO using an optical bench and laser.

2.5. Digital image processing

Developed color negatives (unmounted filmstrips) were converted into digital, true-color (24 bit) bitmaps (1600×1200 pixels in BMP format) using a Polaroid Sprintscan 35^{TM} film scanner. We scanned the photos directly into Adobe Photoshop^{TM} so that all four of the film exposures taken at a single site could be closely compared with the uncompressed TIFF image captured at the same location using the Nikon Coolpix 950. Only the film exposure with a similar level of brightness and contrast as the digital photo was saved for analysis. In total, we kept 48 of the 192 Nikon F images for analysis.

A total of 240 canopy photos (48 film and 192 digital: 48 TIFF, 48 FINE, 48 XGA, and 48 VGA) were analyzed for canopy openness, L_e, and percent-transmitted global PAR using the gap light analyzer (GLA), Version 2.0.4, image processing software (Frazer et al., 1999, 2000b). Canopy openness (the complement of canopy closure) is a sine-weighted measure that represents the relative amount of unobstructed (open) sky visible from a single point in the understory (Jennings et al., 1999; Frazer et al., 2000a); L_e is one-half the total "effective" stand leaf area (m^2) per unit of ground surface area (m^2) (Welles and Norman, 1991); and, percent-transmitted global PAR is the percentage of seasonal, above-canopy global (direct and diffuse) PAR incident beneath the canopy (Canham, 1988). All three measures are dependent on the size, frequency, and distribution of the recorded canopy gaps.

We used the best-fit calibration data determined for the Nikon Coolpix 950, and a polar projection and 180° FOV for the Nikon F to divide the digital and film photos into 10° intervals of zenith and azimuth angle (324 sky regions). Binary classes of sky and canopy pixels were created for each canopy photo by splitting the 24 bit color image into individual RGB planes, and then designating an intensity threshold (0–255) for one or all of the planes (intensities at or below the threshold are considered to be foliage (black), while those above are classified as sky (white)). This process was entirely subjective. First, each red (R), green (G),

and blue (B) plane was examined separately to determine which gave the best gray-scale contrast between sky and canopy. If the contrast did not improve in any of the individual color planes, then the complete RGB (master) image was used for classification. Second, a single threshold intensity, which best suited all regions of the image, was determined for each of the selected R, G, B, or master images; this was done for all 96 uncompressed film (BMP) and digital (TIFF) images. Finally, because the threshold process is a subjective one, the entire procedure was repeated twice more, and the mean of the three threshold values was used to compute canopy openness, L_e, and percent-global PAR for each of the images. We used the identical mean threshold determined for each of the uncompressed TIFF images to analyze the corresponding subset of FINE, XGA, and VGA image formats.

2.6. Statistical analysis

Of the 96 (48 film + 48 digital) uncompressed images processed, we removed a total of 24 images from the final analyses: 3 photos taken in the mature stand were removed due to image defects (appearance of solar disk); 3 photos were discarded from the immature stand data because they formed extreme outliers (photos were taken under large gaps created by deciduous leaf drop); and the other 18 were removed to balance the dataset. The remaining 72 images were stratified into distinct groups based on film type (digital or film), sky type (clear or overcast), and maturity class (immature or mature).

We used the following statistical procedures to analyze our data: (i) Pearson's correlation and linear regression to assess the relationship between digital and film measures of openness, L_e, and global PAR; (ii) paired *t*-tests to identify mean differences between digital and film canopy estimates, as well as between uncompressed and compressed digital photos; (iii) two-way analysis of variance (ANOVA) to study the effects and interaction of stand maturity and sky conditions on digital-to-film ratios of openness, L_e, and global PAR; and (iv) non-linear regression to model radial lens distortion. We tested our data for normality using a normal probability plot and linear best-fit line before running the paired *t*-test and ANOVA statistical procedures. Non-normal data were transformed using either a logarithmic or square root transformation. All statistical analyses were performed at the 5% probability level using SYSTAT Version 8.0, Copyright SPSS Inc., 1998.

3. Results

3.1. Quantitative differences between digital and film photography

3.1.1. Linear relationships between digital and film results

In general, measures of canopy openness, L_e, and transmitted global PAR produced using the digital camera had a significant positive correlation with results obtained using conventional film photography ($R^2 = 0.63$, 0.40, and 0.56, respectively, $n = 36$, $P < 0.001$; Fig. 1). However, the strength of the correlation was generally limited, and varied markedly when these attribute data were stratified into individual maturity classes and sky conditions. For example, digital- and film-derived measures of canopy openness were least correlated in the immature stand under overcast skies ($R^2 = 0.02$, $n = 9$, $P = 0.72$), while R^2 was highest in the mature stand when the sky conditions were also overcast ($R^2 = 0.94$, $n = 9$, $P < 0.001$). The digital and film datasets were generally better correlated in the more open mature stand ($R^2 = 0.55$, $n = 18$, $P < 0.001$) compared to the dense immature stand ($R^2 = 0.06$, $n = 18$, $P = 0.32$). Digital and film measures of canopy openness were also better correlated under overcast skies ($R^2 = 0.79$, $n = 18$, $P < 0.001$) than under clear-sky conditions ($R^2 = 0.59$, $n = 18$, $P < 0.001$). Similar correlation patterns were also found for L_e and transmitted global PAR.

3.1.2. Stand estimates of mean openness, L_e, and transmitted global PAR

For each of the four separate age-by-sky groups (immature × clear, immature × overcast, mature × clear, mature × overcast), we computed stand means and standard errors for digital and film estimates of openness, L_e, and transmitted global PAR (Table 2). Between and within camera comparisons of these data revealed four main differences in the magnitude and range of stand estimates produced by the two camera systems. First, mean estimates of openness derived using the digital camera were larger than the

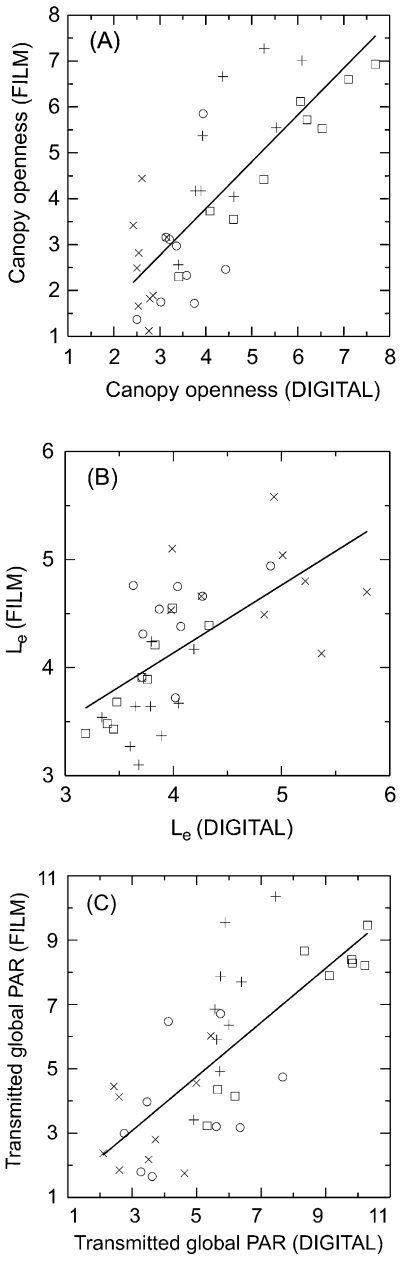

Fig. 1. Scatterplots and linear best-fit (least-squares) lines for comparisons of digital and film-based measures of (A) percent-canopy openness ($Y = -0.290 + 1.019X$, $R^2 = 0.633$, $P < 0.001$); (B) L_e ($Y = 1.622 + 0.628X$, $R^2 = 0.404$, $P < 0.001$); (C) percent-transmitted global PAR ($Y = 0.577 + 0.840X$, $R^2 = 0.562$, $P < 0.001$). Symbols represent the different combinations of maturity class and sky conditions at the time of exposure: (○) immature and clear; (×) immature and overcast; (+) mature and clear; (□) mature and overcast.

film camera in three of four age-by-sky groups; however, the P-value associated with these differences was only significant ($P < 0.05$) in the mature stand under overcast skies. Second, the standard errors were markedly larger for mean openness data extracted from the film photos compared to the digital photos (this was most evident for the immature stand). Third, there were significant differences in mean openness and transmitted global PAR computed from replicate digital camera photos taken under clear and overcast skies; however unlike the film photos, these between sky differences did not reveal any consistent bias. Lastly, mean L_e estimates produced by the film camera were consistently lower in replicate photos taken under clear skies as compared to overcast skies.

3.1.3. Digital-to-film ratios of openness, L_e, and transmitted global PAR

For 22 (61%) of the total 36 digital and film image pairs analyzed, the digital camera produced openness estimates that were, on average, 1.42 ± 0.08 (mean ± S.E.) times larger than the film images. Film openness, on the other hand, exceeded the digital photo estimates in the remaining 14 image pairs by an average of only 1.24 ± 0.06 times. As a result, digital photo estimates of L_e in 23 of the 36 image pairs were, on average, 0.911 ± 0.01 times lower than film measures. For the other 13 image pairs, the mean L_e derived from digital photos was 1.11 ± 0.03 times higher than film. Finally, digital photo estimates of transmitted global PAR were, on average, 1.52 ± 0.09 times greater in 20 (56%) of the 36 image pairs, whereas film photo estimates exceeded digital results by an average of 1.29 ± 0.03 times for the remaining 16 photo pairs.

An ANOVA demonstrated that influences of maturity class and sky conditions on the magnitude and variance of the digital-to-film ratios were slightly different for measures of canopy openness, L_e, and transmitted global PAR. For example, only a moderately significant ($F = 3.303$, d.f. $= 32$, $P = 0.079$) maturity-class difference was noted for canopy openness: the mean digital-to-film openness ratio was larger in the immature stand (1.34 ± 0.125) compared to the mature stand (1.044 ± 0.052). Although sky conditions appeared to have little direct effect ($F < 0.383$, d.f. $= 32$, $P > 0.54$) on any of the digital-to-film ratios, there was a significant to moderately significant ($F > 3.5$, d.f. $= 32$, $P < 0.071$)

Table 2
Summary of mean canopy openness, L_e, and transmitted global PAR extracted from digital and fisheye photographs taken in immature and mature stands under overcast and clear skies

Variable	Sky	Stand	Digital[a]		Film		n
			Mean	S.E.[b]	Mean	S.E.[b]	
Openness	Overcast	Immature	2.682[c]	0.076	2.536	0.345	9
	Clear	Immature	3.436[c]	0.189	2.747	0.444	9
	Overcast	Mature	5.660[c,d]	0.475	4.989[d]	0.523	9
	Clear	Mature	4.540[c]	0.304	5.200	0.531	9
L_e	Overcast	Immature	4.821[c]	0.210	4.781[c]	0.139	9
	Clear	Immature	4.026[c,d]	0.129	4.441[c,d]	0.136	9
	Overcast	Mature	3.681[d]	0.116	3.881[c,d]	0.142	9
	Clear	Mature	3.777	0.084	3.627[c]	0.126	9
Global PAR	Overcast	Immature	3.556[c]	0.408	3.344	0.498	9
	Clear	Immature	4.732[c]	0.557	3.854	0.607	9
	Overcast	Mature	8.309[c,d]	0.680	6.957[d]	0.782	9
	Clear	Mature	5.919[c]	0.232	6.989	0.724	9

[a] Uncompressed, full-resolution (1600 × 1200 pixel) TIFF format.
[b] Standard error of the mean (standard deviation divided by the square root of n).
[c] Significant ($P < 0.05$) within camera and within stand differences due to sky conditions.
[d] Significant ($P < 0.05$) within stand and within sky condition differences due to camera type.

interaction between maturity class and sky type that strongly influenced the variation in canopy openness, L_e, and transmitted global PAR.

3.2. Image resolution and JPEG compression

We compared canopy openness, L_e, and transmitted global PAR extracted from full-resolution (1600 × 1200 pixels), uncompressed TIFF digital photos with replicate datasets obtained from low-compression (1:4) JPEG images in FINE (1600 × 1200 pixels), XGA (1024 × 768 pixels), and VGA (640 × 480 pixels) resolutions (Fig. 2). Although there were no significant mean differences ($t > -1.105$ and $t < 0.440$, d.f. = 26, $P > 0.279$) between the TIFF and FINE digital formats for any of the canopy measures, there were still a number of FINE images that were noticeably different from the original uncompressed TIFF results. For example, the maximum difference in canopy openness, L_e, and transmitted global PAR between TIFF and FINE photos was 0.44%, 0.36 m^2/m^2, and 1.15%, respectively.

All of the mean structural measures computed using the JPEG-compressed (1:4), lower-resolution XGA and VGA formats were significantly different ($t > 2.528$ and $t < -3.705$, d.f. = 26, $P < 0.018$) from the original TIFF images. Both XGA ($3.39 \pm 0.21\%$) and VGA ($3.45 \pm 0.21\%$) images produced a slightly lower ($t > 3.82$, d.f. = 26, $P < 0.001$) mean openness than the TIFF images ($3.55 \pm 0.21\%$). Consequently, mean L_e was slightly higher ($t < -3.71$, d.f. = 26, $P < 0.001$) in XGA ($4.36 \pm 0.15\ m^2/m^2$) and VGA ($4.33 \pm 0.14\ m^2/m^2$) images compared to the full-resolution, uncompressed photos ($4.21 \pm 0.15\ m^2/m^2$). Significant mean differences ($t > 2.53$, d.f. = 26, $P < 0.018$) were also noted for transmitted global PAR estimates extracted from XGA and VGA images: both XGA ($4.45 \pm 0.31\%$) and VGA ($4.54 \pm 0.32\%$) mean estimates were lower than the TIFF photos ($4.74 \pm 0.30\%$). The maximum difference in openness, L_e, and transmitted global PAR, as a result of JPEG compression and the reduced spatial resolution of the XGA and VGA formats, was 0.59%, 0.83 m^2/m^2, and 1.68%, respectively.

3.3. Radial lens distortion and image alignment

All of the radial calibration data[4] determined for the digital camera using the four separate techniques

[4] Calibration data only applies when the Nikon Coolpix 950 is set in M-REC and FISHEYE1 mode.

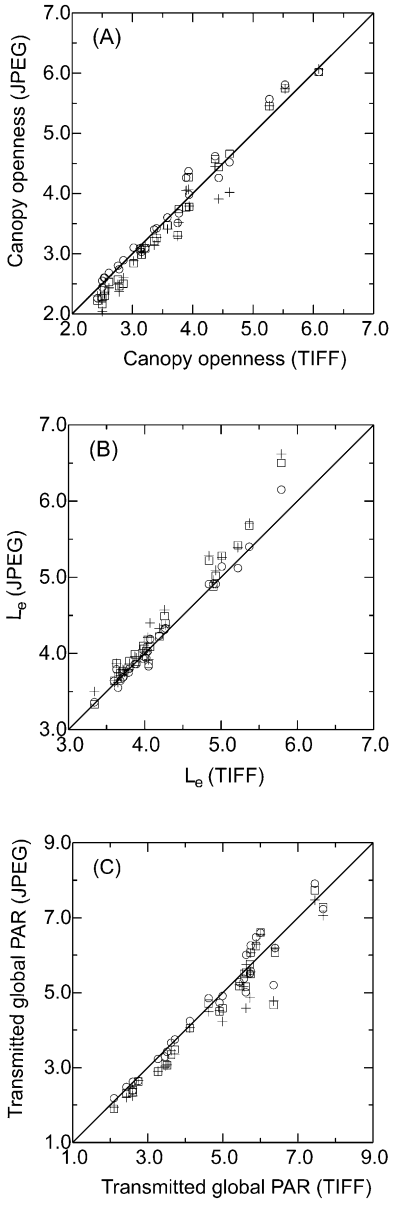

Fig. 2. Combined impact of 1:4 JPEG compression and reduced image resolution on estimates of (A) percent-canopy openness; (B) L_e; (C) percent-transmitted global PAR. The solid-line running diagonally through the data points represents a 1:1 correspondence with a full-resolution (1600 × 1200 pixels), 24 bit uncompressed TIFF image. Symbols represent the different image resolutions of the compressed JPEGs: (○) FINE (1600 × 1200 pixels); (+) XGA (1024 × 768 pixels); and (□) VGA (640 × 480 pixels).

were highly correlated, revealing a non-linear pattern of distortion that could be approximated by a third-order polynomial ($R^2 = 0.9999$, $n = 92$, $P < 0.0001$):

$$Y = 6.6380X - 0.0025X^2 - 2.4014\mathrm{E} - 0.5X^3, \quad 0^\circ \leq X \leq 90^\circ \tag{1}$$

where, Y is the radial position of a projected point measured in pixels from the optical centre of a full-resolution (1600 × 1200 pixels) digital image, and X is the angular distance (°) from the lens' optical axis to a point located in the hemispherical object region. These calibration data also indicate that objects located 90° from the lens' optical axis will be projected to a point 560 pixels from the image centre. Since the full radius of the image is 588 pixels (±2 pixels), we therefore know that the digital camera has a maximum angular FOV that is significantly greater than 180°. Radial distortion results determined for the film camera showed that the Nikkor 8 mm *f*/8 fisheye produced a near-perfect linear (equidistant) radial distortion through its full 180° FOV (Fig. 3).

To test the validity of our radial lens distortion data, we measured and compared the angular coordinates of 60 unique control points identified on 12 separate digital and film image pairs. Control points consisted of prominent branch and stem intersections, shoot tips, and small gaps found randomly distributed within

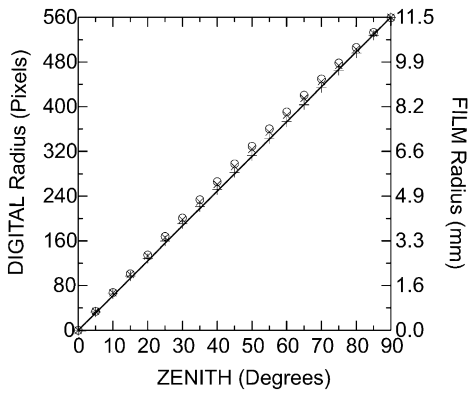

Fig. 3. Radial calibration data measured for the Nikkor 8 mm *f*/8 fisheye lens (+), the Nikon Coolpix 950 and FC-E8 fisheye converter (×), and the well-documented Nikkor 8 mm *f*/2.8 (○), which replaced the older Nikkor 8 mm *f*/8 lens c. 1970. The straight line represents a perfect polar (equiangular) projection.

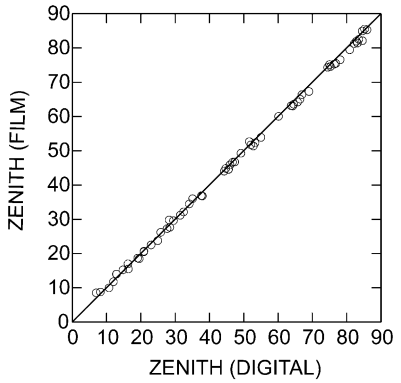

Fig. 4. Scatterplot of unique control points established on 12 digital and film image pairs. The straight line indicates a perfect 1:1 correspondence in the zenith positions of the digital and film control points. Variation in the scatter of these measurements around the 1:1 line is due to the fact that both cameras were not perfectly level at the time of exposure.

each of the image pairs. Regression showed that these common control points had almost identical radial positions (measured in degrees of zenith) when the appropriate projection transformation functions were applied to each of the camera systems ($R^2 = 0.999$, $P < 0.001$, $Y = 0.290 + 0.984X$; Fig. 4). The mean angular difference in the radial positions of all 60 points was only $0.78 \pm 0.07^\circ$ S.E. Angles of azimuth (degrees of rotation in the horizontal plane) were also determined for these same 60 image control points. These data showed that there was a mean angular difference of $2.83 \pm 0.33^\circ$ S.E. in the rotational alignment of the digital and film cameras at the time of exposure.

4. Discussion

Our findings indicate that, despite the significant positive correlation between digital and film photographic estimates of canopy openness, L_e, and transmitted global PAR, there were substantial quantitative differences in the results produced by these two camera systems. Digital and film measures of canopy openness were found to be better correlated under more open forest canopies, as well as under overcast sky conditions. However, the digital camera produced mean L_e estimates that were significantly lower in half of the age-by-sky groups. Mean digital-to-film ratios of openness were higher in the immature stand compared to the more open mature stand; however, the magnitude of this difference was strongly dependent on whether the sky conditions were clear or overcast at the time of exposure. Small angular differences in the corrected radial positions of control points located on digital and film image pairs indicated that the geometric (radial) projection distortion and FOV of the camera optics had little to do with the disparity between digital and film estimates of canopy openness.

4.1. Qualitative differences in image quality

4.1.1. Image sharpness

The most striking visual difference between the digital and film canopy photographs was that the sharpness of the digital images was generally poor compared to the film camera. Consequently, the digital photos appeared blurred, and many of the fine structural details of the canopy were poorly defined. This was particularly evident in areas of high-contrast (i.e. outside edges of stems, branches, and shoots; and the inside edges of canopy gaps). We noted two other unusual characteristics related to blurring in the digital photos. First, image sharpness was not uniform across the entire image, but instead declined with increased radial distance away from the image centre: blurring was most significant at zenith angles greater than 45°. Second, there were distinct color halos present around the high-contrast edges of canopy openings (gaps). The size of these halos increased with increased zenith angle, and they also exhibited a significant spectral and spatial bias. Under clear skies, blue halos formed along the edge of canopy gaps on the side furthest away from the image centre, while green halos appeared on the opposite side of these same gaps (the edge closest to the image centre). Interestingly, blue-colored halos in clear-sky photos were violet under uniformly overcast skies.

4.1.2. Chromatic aberration and color blur

All optical systems are subject to a number of imperfections that prevent a point located in the object region from forming a point on the image plane (Welford, 1986). The spatial and spectral image defects created as a consequence of these imperfections are commonly known as lens aberrations. Chromatic aberration (color blur) is one specific defect that

occurs when full-spectrum (white) light splits into separate wavelengths as it passes through the lens optics: shorter (blue) wavelengths are brought to focus closer to the lens than longer (red) wavelengths (Williams and Becklund, 1972). As a result, multiple color images (halos) are formed simultaneously, each distinct and spatially separated by horizontal distance (longitudinal chromatic aberration) and size (lateral chromatic aberration). Optical designers often use an *achromatic doublet* and anti-reflection coatings to bring blue and red into focus at the same distance; however, a third (or more) lens and lens material (*superachromatic*) is required to correct for green (Ray, 1994).

In our study, the shift of the blue aberration (halo) to violet (blue and red) under overcast skies indicated that the optics of the digital camera was corrected for blue and red but not green wavelengths. The chromatic aberration we detected was therefore the result of the spatial separation and partial overlap of two distinct color images (violet and green). The color shift between blue and violet for the blue aberration occurred because light passing through the canopy gaps was dominated by either blue (clear skies) or by equal intensities of red, green, and blue (overcast skies) wavelengths. Under partly clear skies, each canopy gap exhibited either a uniquely blue or violet aberration, depending on whether the gap had transmitted light scattered from blue sky or cloud. Color blur became more prominent away from the image centre due to the increased disparity in the focal distances of violet and green at larger zenith angles. Interestingly, chromatic aberration was detected in wide-angle photos taken without the fisheye converter, so we suspect that the FC-E8 fisheye converter had only compounded this problem.

4.2. Negative effects of chromatic aberration on analytical results

There were three significant negative effects of chromatic aberration on our digital photographic estimates of canopy structure: (i) the reduced color contrast between sky and canopy elements made accurate and consistent edge detection impossible; (ii) color blur created spatial artifacts that simplified the shape and modified the size of canopy gaps; and (iii) lateral chromatic aberration, along with its spectral shift under different sky conditions, interfered with the reliability of the threshold process and the replication of results.

4.2.1. Edge-detection and threshold errors

Overexposure of either digital or film fisheye photographs is known to create substantial error in the amount and distribution of measured canopy openness (Chen et al., 1991, Macfarlane et al., 2000). Blurring caused by excessive light scattering and diffraction along the edges of branches and leaves is considered to be the primary cause of this problem (Chen et al., 1991; Wagner, 1998). Small differences (errors) in the position of the foliage-sky border can therefore lead to proportionately large differences in openness, particularly in canopy photos characterized by numerous small gaps with large perimeter-to-area ratios (Frazer et al., 2000a). The lateral chromatic aberration produced by the digital camera has compounded the blurring problem even further, making accurate and consistent edge detection largely impossible. The negative impact of color blurring on edge detection was most noticeable in the immature stand because of the preponderance of small canopy gaps.

4.2.2. Modification of gap size and shape, and the redistribution of openness

Chromatic aberration created a substantial amount of pixel mixing in the digital photos, and this affected individual canopy gaps in two ways. First, very small gaps were lost during the threshold stage because they appeared darker than other larger gaps (gap brightness was dominated by foliar brightness). Second, other gaps increased in size, and their shapes became more simplified (gap brightness was dominated by sky brightness). We suspect the latter to be the dominant effect because of the larger mean digital-to-film openness ratios (1.42 ± 0.08 S.E.) exhibited by the majority of the digital and film image pairs. Relative differences in the angular (radial) distributions of digital and film canopy openness indicated that color blur had an increased effect on gap size away from the image centre. In general, digital-to-film openness ratios increased with increased angular distance from the zenith (Fig. 5). Although, ratios computed for the immature stand fluctuated markedly over the first 65°, both the clear and overcast datasets showed a dramatic rise after that. In the mature stand, overcast and clear-sky curves follow a slight but steady rise from the image

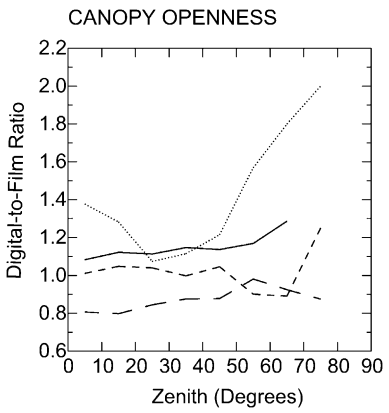

Fig. 5. Angular (radial) distributions of the digital-to-film ratios of canopy openness computed for different maturity and sky class combinations. Patterns of increase are similar in the mature stand under clear and overcast skies. The effects of color blur are less predictable in the immature stand; however, clear and overcast sky curves both show a significant rise at large zenith angles. Different line types represent ratios stratified by maturity and sky class, i.e. dotted (immature and clear); short dash (immature and overcast); long dash (mature and clear); and solid (mature and overcast).

centre to the outer edge. Englund et al. (2000) also found that the Nikon Coolpix 950 produced canopy openness estimates that were significantly larger than film measures; however, these authors suggested that this disparity might have been due to differences in the light sensitivity of digital and film cameras.

4.2.3. Replication of results

Unlike conventional film, the digital camera could not reproduce openness results that were statistically similar when exposed under different sky conditions in either of the two stands (immature: $t = 3.123$, d.f. $= 8$, $P = 0.014$; mature stand: $t = -3.476$, d.f. $= 8$, $P = 0.008$). In addition, digital photos were extremely difficult to threshold, and no single color plane seemed to improve the contrast between sky and canopy elements. Film, on the other hand, was very simple to threshold; the blue plane consistently produced the best color contrast; and openness measurements were easily replicated ($t < 0.912$, d.f. $= 8$, $P > 0.388$).

The inability of the digital camera to produce consistent openness data under different sky conditions was a consequence of two factors. First, color blur obscured the sharp edge between foliage and sky, making accurate and repeatable edge detection difficult. Second, the lateral displacement of violet (red and blue) and green wavelengths into two separate images created significant spatial and spectral (color) biases that varied with the sky conditions. For example, as the dominant wavelength (hue) of the sky changed between clear and overcast days, or even within the same image scene (e.g. a partly cloudy sky), the spectral composition of the violet and green aberrations (halos) would also change. Choosing any one particular RGB color plane to threshold therefore created a unique shift in the range and position of gray-scale intensities that was strongly sky-dependent.

The negative impact of the color bias in chromatic aberration was minimized when digital photos were exposed under overcast skies, mostly because clouds scatter more uniform (equal) intensities of red, green, and blue. Averaging all three RGB planes into a single gray-scale image therefore helped to further minimize this color-bias effect. Partly clear skies had the worst impact on the digital photos because of the enormous variation in the spectral composition of the chromatic aberration, e.g. cloudy regions of the image were dominated by equal portions of red and blue (violet), while blue sky regions produced aberrations that were low in red and saturated in blue. The green plane provided the most consistent range of gray-scale intensities under these sky conditions, because clouds and blue sky scattered similar amounts of green light. Nevertheless, clear or partly clear skies should be avoided, and the Nikon Coolpix 950 should only be used to take black and white photos under uniformly overcast skies.

4.3. Hemispherical photography and uniform overcast skies

One of the drawbacks of exposing digital and film hemispherical photographs under uniformly overcast skies is the intense scattering of diffuse light around the zenith (Chen et al., 1991; Frazer et al., 2000a). In this study, optimizing the exposure to handle the extreme brightness close to the zenith resulted in a significant amount of underexposure at zenith angles greater than 35° (Fig. 6). The steady rise in the ratio of openness computed from overcast photos to openness measured under clear skies also showed that the blurring effect created by light scattering and diffrac-

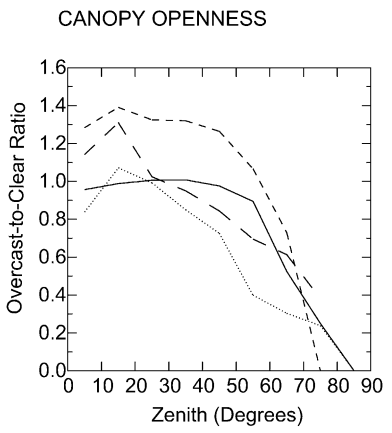

Fig. 6. Angular (radial) distributions of overcast-to-clear-sky ratios of canopy openness indicate that canopy openness measured under clear skies is generally lower close to the zenith and higher close to the horizon relative to canopy openness measured under overcast skies. These distribution curves demonstrate that both digital and film photography are affected by intense diffuse scattering around the zenith on overcast days. Different line types represent ratios stratified by film and sky type, i.e. dotted (digital and immature); short dash (digital and mature); long dash (film and immature); and solid (film and mature).

tion around the edges of leaves and branches was limited to the first 20–30° of zenith angle. Although the overall impact of light scattering on canopy openness was relatively small, the shift in the distribution of openness away from the horizon had significant implications for estimates of L_e. Film measures of mean L_e computed for both the immature and mature stand were significantly larger ($t < -3.866$, d.f. $= 8$, $P < 0.005$) on overcast days even though there were only very small increases in openness ($t < 0.912$, d.f. $= 8$, $P > 0.388$). Interestingly, the low scatter and uniform lighting created by clear skies produced film photos that had superb sharpness and color contrast. Under these conditions, the blue color plane in film photos consistently produced the best gray-scale contrast between sky and canopy elements.

4.4. Considerations for using multi-purpose, consumer-grade digital cameras

4.4.1. Image quality

Consumer-grade digital cameras are designed to be inexpensive and to handle a wide range of focal lengths and fields of view (e.g. wide angle, telephoto, and macro formats). Although these cameras produce images that look good visually, they can contain subtle image defects (aberrations) that will interfere with quantitative measurements and analyses. Certain kinds of residual aberrations (e.g. radial lens distortion) can be easily corrected during image processing. Other optical defects, however, degrade image sharpness and therefore require correction at the optical design stage (e.g. chromatic aberration, coma, astigmatism, and spherical aberration; Williams and Becklund, 1972). Digital camera systems may complicate this problem even further because of other potential added sources of image error produced by the detector (CCD array), supporting electronics, and the digital signal processing (Holst, 1996). We suspect that lens aberrations (mostly chromatic aberration), limited resolution of the CCD (1.92 million pixels), sensor noise, and color interpolation may have all contributed to the diminished image sharpness produced by the Nikon Coolpix 950.

The ability to resolve the fine-scale architecture of canopies is a necessary requirement for accurate photographic (digital or film) measurements of gap size and distribution, particularly in dense closed canopies (less than 10% openness). Although hemispherical photography may not be the best technique to use in these types of stands, it is possible to distinguish subtle qualitative differences in canopy openness in dense canopies (3–10% openness) provided photos are carefully taken using high-quality photographic equipment (e.g. Frazer et al., 2000a). The color blur associated with the Nikon Coolpix 950 has been shown here to impact on (i) gap size, shape, and distribution; (ii) the accuracy and consistency of edge-detection; and (iii) the magnitude, range, and replication of canopy openness results. In general, the Nikon Coolpix 950 produced canopy-openness measures that were 1.4 times greater than film estimates in 22 of the 36 photo pairs. Cloud cover and sky brightness also influence the spectral characteristics of the lateral chromatic aberration (halos), and thus have an added and unpredictable effect on canopy openness. Setting the Nikon Coolpix 950 to record black and white images, and shooting only under uniformly overcast skies will help minimize the unpredictable effects of chromatic aberration. Nevertheless, we do not recommend the use of this camera in closed canopies when openness falls below 10%.

4.4.2. Image storage

Image compression and resampling are two methods utilized by the Nikon Coolpix 950 to minimize the memory requirements for image storage. Joint Photographic Experts Group (JPEG) is a standardized image compression technique that reduces the file size of true-color (RGB) or gray-scale digital images (Pennebaker and Mitchell, 1993). JPEG compression can achieve significant reductions in file size because it permanently discards high-frequency color (chroma) information in discrete blocks of pixels throughout the image (the luminance component of each pixel remains mostly unchanged). Decreasing the JPEG-compression ratio will therefore have an increasingly deleterious effect on image quality (Pennebaker and Mitchell, 1993). Here, we found that 1:4 JPEG compression had no significant influence on mean stand estimates of canopy openness, L_e, or transmitted global PAR; however, because there were certain JPEG images that displayed substantial differences in these variables from the original uncompressed TIFF format, we do not recommend the use of JPEG-compression ratios smaller than 1:4.

Setting the Nikon Coolpix 950 to store photos in XGA and VGA formats reduces the total number of pixels in a single image by factors of 0.41 and 0.16, respectively. There is no option to store XGA or VGA images in an uncompressed format; thus, images archived at either of these two resolutions are also subject to JPEG compression. In this study, the combined impact of 1:4 JPEG compression and the reduced XGA and VGA spatial resolutions produced mean canopy openness estimates that were significantly lower than the full-resolution, uncompressed TIFF images. We suspect that this difference in canopy openness was mostly due to a loss of spatial resolution, whereby the smaller canopy gaps found at larger zenith angles in the full-resolution TIFF photos were no longer preserved in the XGA and VGA formats. Since the JPEG compressor always works in discrete pixel blocks of a fixed size (e.g. 8×8 pixels), we also know that high-frequency color information was removed across different segments of the image for full-size (1600×1200 pixels), XGA (1024×768 pixels), and XGA (640×480 pixels) formats. To avoid both of these potential problems, it is advisable to purchase more compact flash memory (48 Mb or larger) and store images in full-size (1600×1200 pixels) uncompressed TIFF or 1:4 compression JPEG formats only.

4.4.3. Other considerations

Other practical considerations for using digital cameras in forest canopy studies are: (i) these cameras can require a constant supply of batteries, particularly when outdoor temperatures are low (less than 10°C); (ii) data transfer and storage are always a concern because of the significant amount of internal memory required for a single uncompressed image; and (iii) the long-term performance of these cameras under field conditions is largely unknown. Scientific-grade 35 mm fisheye lenses (e.g. 8 or 10 mm (OP) Nikkor) mounted on conventional film cameras or professional digital cameras (e.g. Fournier et al., 1997) can produce excellent high-quality images for analysis; however, their purchase costs are high, and lenses are currently in limited supply since they are no longer being manufactured. Thus, the recent move to consumer-grade digital cameras for canopy research has for many been a necessary one. With technological improvements forthcoming, the future of this digital technology appears promising. Nevertheless, the intended application and use of the photographs must be carefully considered before selecting a photo system for hemispherical canopy photography.

Acknowledgements

We gratefully acknowledge the support of the following individuals and institutions: Ken Lertzman for supplying all of the photographic equipment; Daniel Mailly, Quentin Mackie, and Trevor Orchard for assistance with the fisheye lens calibrations; Bob Ferris for assistance in the field; and the Canadian Forest Service at the Pacific, Northern, and Laurentian Forestry Centers for financial support. We also thank the two anonymous reviewers for excellent suggestions to improve this manuscript.

References

Canham, C.D., 1988. An index of understory light levels in and around canopy gaps. Ecology 69, 1634–1703.

Canham, C.D., Denslow, J.S., Platt, W.J., Runkle, J.R., Spies, T.A., White, P.S., 1990. Light regimes beneath closed canopies and

tree-fall gaps in temperate and tropical forests. Can. J. For. Res. 20, 620–631.

Canham, C.D., Finzi, A.C., Pacala, S.W., Burbank, D.H., 1994. Causes and consequences of resource heterogeneity in forests: interspecific variation in light transmission by canopy trees. Can. J. For. Res. 24, 337–349.

Chazdon, R.L., Field, C.B., 1987. Photographic estimation of photosynthetically active radiation: evaluation of a computerized technique. Oecologia (Berlin) 73, 525–532.

Chen, J.M., Black, T.A., Adams, R.S., 1991. Evaluation of hemispherical photography for determining plant area index and geometry of a forest stand. Agric. For. Meteorol. 56, 129–143.

Clark, J.A., Follin, G.M., 1988. A simple "equal area" calibration for fisheye photography. Agric. For. Meteorol. 44, 19–25.

Englund, S.R., O'Brien, J.J., Clark, D.B., 2000. Evaluation of digital and film hemispherical photography and spherical densiometry for measuring forest light environments. Can. J. For. Res. 30, 1999–2005.

Fournier, R.A., Rich, P.M., Landry, R., 1997. Hierarchical characterization of canopy architecture for boreal forests. J. Geophys. Res. 102, 29445–29454.

Frazer, G.W., Trofymow, J.A., Lertzman, K.P., 1997. A method for estimating canopy openness, effective leaf area index, and photosynthetically active photon flux density using hemispherical canopy photography and computerized image analysis techniques. Can. For. Ser., Pac. For. Cent., Inf. Rep. no. BC-X-373.

Frazer, G.W., Canham, C.D., Lertzman, K.P., 1999. Gap Light Analyzer (GLA), Version 2.0: Imaging software to extract canopy structure and gap light transmission indices from true-color fisheye photographs. Copyright 1999: Simon Fraser University, Burnaby, BC, and the Institute of Ecosystem Studies, Millbrook, New York; (http://www.rem.sfu.ca/forestry/index.htm or http://www.ecostudies.org).

Frazer, G.W., Trofymow, J.A., Lertzman, K.P., 2000a. Canopy openness and leaf area in chronosequences of coastal temperate rainforests. Can. J. For. Res. 30, 239–256.

Frazer, G.W., Canham, C.D., Lertzman, K.P., 2000b. Gap light analyzer (GLA), Version 2.0: image-processing software to analyze true-color, hemispherical canopy photographs. Bull. Ecol. Soc. Am. 81, 191–197.

Gendron, F., Messier, C., Comeau, P.G., 1998. Comparison of various methods for estimating the mean growing season percent photosynthetic photon flux density in forests. Agric. For. Meteorol. 92, 55–70.

Gray, A.N., Spies, T.A., 1996. Gap size, within-gap position and canopy structure effects on conifer seedling establishment. J. Ecol. 84, 635–645.

Green, R.N., Klinka, K., 1994. A field guide to site identification and interpretation for the Vancouver Forest Region. Min. For., Victoria, BC, Land Manage. Handbook no. 28.

Herbert, T.J., 1987. Area projections of fisheye photographic lenses. Agric. For. Meteorol. 39, 215–223.

Holst, G.C., 1996. CCD arrays, cameras, and displays. SPIE Optical Engineering Press, Winter Park, FL, 332 pp.

Jennings, S.B., Brown, N.D., Sheil, D., 1999. Assessing forest canopies and understorey illumination: canopy closure, canopy cover, and other measures. Forestry 72, 59–73.

Macfarlane, C., Coote, M., White, D.A., Adams, M., 2000. Photographic exposure affects indirect estimation of leaf area in plantations of *Eucalyptus globulus* Labill. Agric. For. Meteorol. 100, 155–168.

Nicotra, A.B., Chazdon, R.L., Iriarte, S., 1999. Spatial heterogeneity of light and woody seedling regeneration in tropical wet forests. Ecology 80, 1908–1926.

Parker, G.G., 1995. Structure and microclimate of forest canopies. In: Lowman, M.D., Nadkarni, N.M. (Eds.), Forest Canopies. Academic Press, Orlando, FL, pp. 73–98.

Pennebaker, W.B., Mitchell, J.L., 1993. JPEG Still Image Data Compression Standard. Van Nostrand Reinhold Press, New York, NY, 650 pp.

Perry, D.A., 1994. Forest Ecosystems. John Hopkins University Press, Baltimore, MA, 649 pp.

Ray, S.F., 1994. Applied Photographic Optics: Lenses and Optical Systems for Photography, Film, Video, and Electronic Imaging. Focal Press, Oxford, UK, 586 pp.

Rich, P.M., 1990. Characterizing plant canopies with hemispherical photographs. Remote Sens. Rev. 5, 13–29.

Spies, T.A., 1998. Forest structure: a key to the ecosystem. Northwest Sci. 72, 34–39.

Trofymow, J.A., Blackwell, B.A., Porter, G.L., Marshall, V., Arsky, R., Pollard, P., 1997. An establishment report on chronosequences selected for research into the effects of converting coastal British Columbia old-growth forests to managed forests. Can. For. Ser., Pac. For. Cent., Info. Rep. no. BC-X-374.

Wagner, S., 1998. Calibration of grey values of hemispherical photographs for image analysis. Agric. For. Meteorol. 90, 103–117.

Welford, W.J., 1986. Aberrations of Optical Systems. Adam Hilger Ltd., Bristol, UK.

Welles, J.M., Cohen, S., 1996. Canopy structure measurement by gap fraction analysis using commercial instrumentation. J. Exp. Bot. 47, 1335–1342.

Welles, J.M., Norman, J.M., 1991. Instrument for indirect measurement of canopy structure. Agron. J. 83, 818–825.

Williams, C.S., Becklund, O.A., 1972. Optics: A Short Course for Engineers and Scientists. Wiley/Interscience, New York, USA, 397 pp.

Wright, E.F., Coates, K.D., Canham, C.D., Bartemucci, P., 1998. Species variability in growth response to light across climatic regions in northwestern British Columbia. Can. J. For. Res. 28, 871–886.